Journal of Hazardous Materials 192 (2011) 500–506

Contents lists available at ScienceDirect

Journal of Hazardous Materials

journal homepage: www.elsevier.com/locate/jhazmat

Synthesis of granular activated carbon/zero valent iron composites for simultaneous adsorption/dechlorination of trichloroethylene

Hui-Hsin Tseng[a,b], Jhih-Gang Su[c], Chenju Liang[c,*]

[a] School of Occupational Safety and Health, Chung Shan Medical University, Taichung 402, Taiwan
[b] Department of Occupational Medicine, Chung Shan Medical University Hospital, Taichung 402, Taiwan
[c] Department of Environmental Engineering, National Chung Hsing University, 250 Kuo-Kuang Rd., Taichung City 402, Taiwan

ARTICLE INFO

Article history:
Received 2 March 2011
Received in revised form 12 May 2011
Accepted 16 May 2011
Available online 23 May 2011

Keywords:
Reactive activated carbon
Chlorinated solvent
Reduction
Groundwater remediation
Waste water treatment

ABSTRACT

The coupling adsorption and degradation of trichloroethylene (TCE) through dechlorination using synthetic granular activated carbon and zerovalent iron (GAC–ZVI) composites was studied. The GAC–ZVI composites were prepared from aqueous Fe^{2+} solutions by impregnation with and without the use of a PEG dispersant and then heated at 105 °C or 700 °C under a stream of N_2. Pseudo-first-order rate constant data on the removal of TCE demonstrates that the adsorption kinetics of GAC is similar to those of GAC–ZVI composites. However, the usage of GAC–ZVI composites liberated a greater amount of Cl than when ZVI was used alone. The highest degree of reductive dechlorination of TCE was achieved using a GAC–ZVI700P composite (synthesized using PEG under 700 °C). A modified Langmuir–Hinshelwood rate law was employed to depict the behavior of Cl liberation. As a result, a zero-order Cl liberation reaction was observed and the desorption limited TCE degradation rate constant decreased as the composite dosage was increased. The GAC–ZVI composites can be employed as a reactive GAC that is not subject to the limitations of using GAC and ZVI separately.

1. Introduction

Activated carbon (AC) adsorption technology is most oftenly used for the urgent removal of persistent organic pollutants from an aqueous phase (e.g., groundwater) or from a gaseous phase (e.g., extracted contaminated soil vapors). However, this process achieves phase transfer only and not decomposition of contaminants. Therefore, this study aims to produce a reactive AC for environmental remediation, which will overcome the limitations of AC adsorption. With the recent development of nanotechnology, nanoscale zero valent iron (nZVI) particles have been successively synthesized and, due to their great capacity for reductive reaction, display great potential for future usage in the remediation of environmental contaminants [1,2].

The reactivity of nZVI is mainly due to its high specific surface area [1]. However, bare nZVI particles (30–100 nm) exhibit a strong tendency to agglomerate because of their high surface energies and intrinsic magnetic interactions [3]. While the chemistry of the dechlorination of chlorinated solvents such as trichloroethylene (TCE) by nZVI has been extensively studied [4,5], there are still some properties of nZVI, which reduce its effectiveness in reductive reactions and there are technical challenges associated with its use [6]. For example, when exposed to air, nZVI is rapidly oxidized and loses its high reactivity. Furthermore, nZVI particles tend to agglomerate into particles of over 10 μm, which results in the decrease of surface area, mobility and reactivity [3,6–10]. These characteristics may reduce the effectiveness of nZVI in reducing pollutants. In order to prevent aggregation, supporting nZVI on silica [3], graphite [9], various membranes [11,12] and palladized iron embedded in AC [13,14] have been researched. Among these supporting materials, AC is the most viable option due to its high sorption capacity, high surface area, porous structure and relatively low cost [15]. AC adsorption can be utilized to retain contaminants in close proximity to the supported ZVI and allow adsorptive and reductive reactions to occur simultaneously. However, a literature survey that we conducted revealed no experimental studies on synthesis and application of bare nZVI coated AC.

To explore the advantages of the combined usage of AC and nZVI and to investigate whether certain factors, which limit their application when individually used and this could be overcome, granular AC (GAC) coated with nZVI was synthesized. The physical adsorption capacity of GAC was combined with the dechlorination destructive reactivity of nZVI to produce a reactive AC. Since the dispersant is capable of creating a stable dispersion of ZVI nanoparticles [16] and the elevated calcination temperature may remove surface functional groups on GAC [17] and increase diffusion rate of iron in pores of GAC [18], the influences of the temperature

* Corresponding author. Tel.: +886 4 22856610; fax: +886 4 22862587.
E-mail address: cliang@dragon.nchu.edu.tw (C. Liang).

0304-3894/$ – see front matter © 2011 Elsevier B.V. All rights reserved.
doi:10.1016/j.jhazmat.2011.05.047

of calcination and of the dispersant used during the synthesizing process were evaluated. The characterization of the GAC–ZVI composites was also investigated. The influences of the temperature of calcination and of the dispersant used during the synthesizing process were evaluated and the characterization of the GAC–ZVI composites was investigated. Moreover, the mechanistic aspects of the combined adsorption and dechlorination of TCE were compared to those of the separate adsorption and dechlorination of TCE.

2. Experimental

2.1. Materials and chemicals

All water used was purified using a Millipore reverse osmosis (RO) purification system. A commercial activated carbon Calgon Filtrasorb 400 (F400) (which uses bituminous-coal-based carbon) was obtained from the Calgon Carbon Corporation. All of the AC used (particles sieved: 1.2–2.0 mm) in this experiment was prepared by acid washing with 5% HCl for 24 h to remove any impurities present and then rinsed with RO water until the pH of the solution stabilized. The AC was then dried at 105 °C for 24 h prior to storage in a desiccator. Ferrous sulfate heptahydrate (98–102.5%, Union Taiwan), sodium borohydride (>95%, Riedel-deHaën), polyethylenglykol 4000 (PEG-4000, Fluka) and sulfuric acid (>99.8%, Fluka) were used for synthesis of the GAC–ZVI composites. Methanol (99.9%, ECHO) was used in the preparation of a series of trichloroethylene (>99.5%, Fluka) standard solutions. nPentane (99.9%, Fluka) was used for the extraction of the TCE solution. Sodium chloride (99.8%, Riedel-deHaën), sodium carbonate (99.5–100.5%, Riedel-deHaën) and sodium bicarbonate (99.7%, Riedel-deHaën) were used for chloride analysis. Nitric acid (>65%, Fluka), hydrochloric acid (min. 37%, Merck) and sodium hydroxide (min. 99%, Riedel-deHaën) were used for the digestion of the synthetic composites. The FerroVer Iron and ferrous Iron reagents, used for analyzing total iron and ferrous ion, respectively, were purchased from Hach.

2.2. Synthesis of GAC/nZVI composites

In this work, the nZVI was prepared using a traditional reduction method whereby a strong reducing agent (i.e., $NaBH_4$) was used to reduce Fe^{2+} to nZVI (see Eq. (1) [19,20]). The dispersant employed was PEG-4000 based on the methodology of Ghauch et al. [21]. The procedure for synthesizing GAC–ZVI is briefly described as follows. In accordance with the methodology of Fan et al. [22], the applied iron dosage used in these experiments was approximately 40 mg Fe g^{-1} GAC. In the experiments, which were designed to examine the effects of the dispersant, 0.5 g of PEG was dissolved in 100 mL of ferrous sulfate solution [20]. Thereafter, 10 g of GAC was added to a 150 mL beaker containing 100 mL of the prepared iron solution and the resulting slurry was mixed in an ultra-sonic bath (Ultrasonic Cleaner, Model: Delta DC150) for 2 h and then further shaken for 48 h on a reciprocating shaker at 200 rpm (IKA HS 260) (note: nitrogen purging was conducted during mixing). The iron-impregnated GAC, which was sieved through a #30 mesh sieve (openings of 0.6 mm) by hand, was added slowly to 500 mL of 1.0 M $NaBH_4$. After a 2 h reaction, the GAC–ZVI composites formed were filtered and washed using first degassed RO water, then acetone, and finally with degassed RO water. This washing process was carried out for a minimum of three cycles. The whole process was conducted in a nitrogen atmosphere. Following washing, the GAC–ZVI composites were dried at 105 °C for 24 h under a stream of N_2 at 500 mL min^{-1} before being heated at an increased rate of 13.5 °C min^{-1} to a final temperature of 700 °C (Tube furnace, Model: CF-66, Chung Chuan Ltd.) which was maintained for 30 min (process modified after Sun et al. [23]). The synthesized GAC–ZVI composites were then placed in a covered bottle filled with N_2 and stored at room temperature until needed.

$$Fe^{2+} + 2BH_4^- + 6H_2O \rightarrow Fe^0 + 2B(OH)_3 + 7H_2 \quad (1)$$

2.3. TCE adsorption/dechlorination experiment

The concentration of TCE solution (80 mg L^{-1}) was prepared by adding the required amount of pure TCE to a 1.36 L heavy-walled plain pressure reaction flask (IWAKI 7740 glass) with no headspace and stirring overnight. The flask was placed in a temperature-controlled chamber at 20 °C and the top of the flask was covered and clamp-sealed with a flat Teflon reaction head. The pH and ORP probes used were inserted through Teflon-lines septum ports in the reaction head. A gas-tight syringe was used to withdraw 5.0 mL of the solution through a septum port for analyzing the TCE and Cl contents. Two sets of experiments on adsorption and/or dechlorination of TCE using ZVI, GAC, and GAC–ZVI composites were conducted. The first set of experiments used a shorter reaction period (i.e., 360 min), and 5 g L^{-1} of GAC or GAC–ZVI composites were added in the reaction flask while 0.15 g L^{-1} ZVI was added based on 5 g L^{-1} composite × approximate 3% iron content. In the other set of experiments, a longer reaction time (i.e., 10 d) was used, and 5, 8, or 10 g L^{-1} GAC–ZVI composites were employed.

2.4. Analysis

The surface area and porosity of the composite samples were measured using a nitrogen sorption technique at 77 K (Micrometritics ASAP 2020, high surface area and porosimetry analyzer). Specific surface areas and pore volumes were determined using the Brunauer–Emmett–Teller (BET) and Barrett–Joyner–Halenda (BJH) equations, respectiely. X-ray diffraction (XRD) analysis (MAC Science (MXP18) diffractometer) was conducted to determine the crystal structure and crystallinity of the GAC–ZVI composites. A JOEL JEM-1400 transmission electron microscope (TEM) was used to observe the morphology and crystallographic properties of the composites. A JEOL JSM-6700F scanning electron microscope (SEM), equipped with both secondary electron imaging (SEI) and backscattered electron imaging (BEI) modes, was used to observe the morphology and size of the composites. The SEM was also equipped with an Oxford Inca Energy-400 energy dispersive spectrometer (EDS) for observing chemical composition. Chloride ion analysis was performed using a Metrohm 790 ion chromatograph coupled with a conductivity detector and a Metrosep A Supp 5 column. Total iron and ferrous ion amounts were quantified using 1,10-phenathroline at a wavelength of 510 nm in a Hach DR/2000 spectrophotometer. The pH levels of the sample were measured periodically using a pH electrode and an ORP (Mettler Toledo Inlab®) was recorded continuously at 5 s intervals using CyberScan PC 5000 software (Eutech Instruments). For aqueous TCE analysis, a 2 mL aliquot was placed in a 5 mL brown bottle containing 1.5 mL of pentane and then place on a vortex shaker set at 1400 rpm for 3 min (Thermolyne Type 65800). For analysis of sorbed TCE on the composite, residual AC was filtered and approximately 0.1 g amounts of the composite were weighed and immediately placed in 5 mL brown bottles containing 3 mL of pentane for a subsequent extraction of 5 min on a vortex shaker. The TCE extract was analyzed using a gas chromatography/flame ionization detector (Agilent 6890N) in accordance with the operational conditions outlined by Liang et al. [24].

Table 1
BET surface area and pore volume of the GAC–ZVI composites.

Composite	BET surface area ($m^2\ g^{-1}$)	Cumulative volume ($cm^3\ g^{-1}$)	Pore volume ($cm^3\ g^{-1}$)			Iron content (mg Fe g^{-1} composite)	
			Pore diameter (mm)			Before reaction	After reaction
			<2	2–50	>50		
GAC	930.1	0.249	0.313	0.241	0.008	0	0
GAC–ZVI105	792.9	0.130	0.301	0.123	0.007	26.1	23.3
GAC–ZVI700	782.6	0.152	0.306	0.145	0.007	23.4	25.2
GAC–ZVI105P	780.8	0.203	0.278	0.190	0.013	23.2	19.8
GAC–ZVI700P	826.1	0.193	0.304	0.185	0.008	21.5	21.3

3. Results and discussion

3.1. GAC–ZVI characterization

The GAC–ZVI composites were prepared from aqueous Fe^{2+} solutions by impregnation and then heated at 105 °C or 700 °C under a stream of N_2. The nomenclature GAC–ZVI105 and GAC–ZVI700 was applied to ZVI entrapped in porous GAC and heated to 105 ° and 700 °C, respectively, while GAC–ZVI105P and GAC–ZVI700P represent the composites that were prepared using PEG. The BET surface area of the composites ranged from 782.6 to 826.1 $m^2\ g^{-1}$, which is smaller than that of the GAC starting material (930.1 $m^2\ g^{-1}$) (data presented in Table 1). The ZVI imbedded in the GAC likely contributed to this reduction in BET surface area and also reflects changes that occurred in the porosity of the GAC. The results show that, at all pore volumes and diameters (i.e., pore diameters ranging 2–50 nm), the internal porosity of the mesh pores decreased significantly. These changes likely ensured entry of the $NaBH_4$ solution which then, mainly within the mesopores, reduced Fe^{2+} to generate ZVI and resulted in the disappearance of many of the mesopores. Adsorption around micropores, which are closely surrounded by pore walls, is much stronger than on the relatively flat surfaces of meso- and macropores [25]. However, the micropores in this study remained apparently unaltered, which may suggest that the composites still retained an adsorptive capability. Additionally, the iron contents of the four composites ranged from 21.5 to 26.1 mg Fe g^{-1} composite (Table 1).

Fig. 1 shows the SEM/BEI images of four composites. The images clearly show an even distribution of ZVI throughout the surface of the GAC in the composites that were prepared with the usage of PEG (comparing the white dots in Fig. 1(c and d) to those in Fig. 1(a and b)). The PEG dispersant, due to its natural thermodynamically unstable state, causes to electrostatic repulsion and steric hindrance, which reduces potential ZVI aggregation [26]. Note that the SEM images of ZVI particles prepared without the GAC support and the four composites at different magnifications are presented in Figs. SI1(a) and (b)–(e), respectively. The results of EDS elemental analysis for all four composites are presented in Figs. SI2–SI5 and confirm the presence of two major carbon and iron elements on the surface of the composites. However, even though the usage of PEG resulted in a more uniform distribution of ZVI over the GAC surface, the 50,000× magnification SEM/SEI image shows that the nano-sized ZVI particles had formed into spherical or chainlike structures (see Fig. 1(g and h)). As the temperature of calcination was raised from 105 to 700 °C, more aggregated structures of increased particle size (approximately from ~50 to above 100 nm in diameter) were present in the GAC. Additionally, the use of PEG appears to have resulted in more complete dispersal of the ZVI particles at a higher calcination temperature (i.e., 700 °C) (by comparing Fig. 1(f) to Fig. 1(h)), which was due to the scattering effects of PEG upon encapsulated ZVI [16]. Furthermore, Fig. SI6 shows a TEM image of the GAC–ZVI700P which shows that the composite is comprised of roughly spherical ZVI particles, ~10–100 nm in diameter, which are situated within pores. This indicates that the ZVI particles were more completely dispersed and that particle size had decreased, which contrasts with observations made using the SEM. This is possibly due to the fact that the size of the pores on the GAC regulates the size of the ZVI within the pores [27]. The XRD analysis, presented in Fig. 2, shows that the main reflection occurred at 44.7 (2-theta degree) for nZVI and all GAC–ZVI composites, which is consistent with literatures [6,9,26] and the ZVI prepared in this study without the usage of a GAC support.

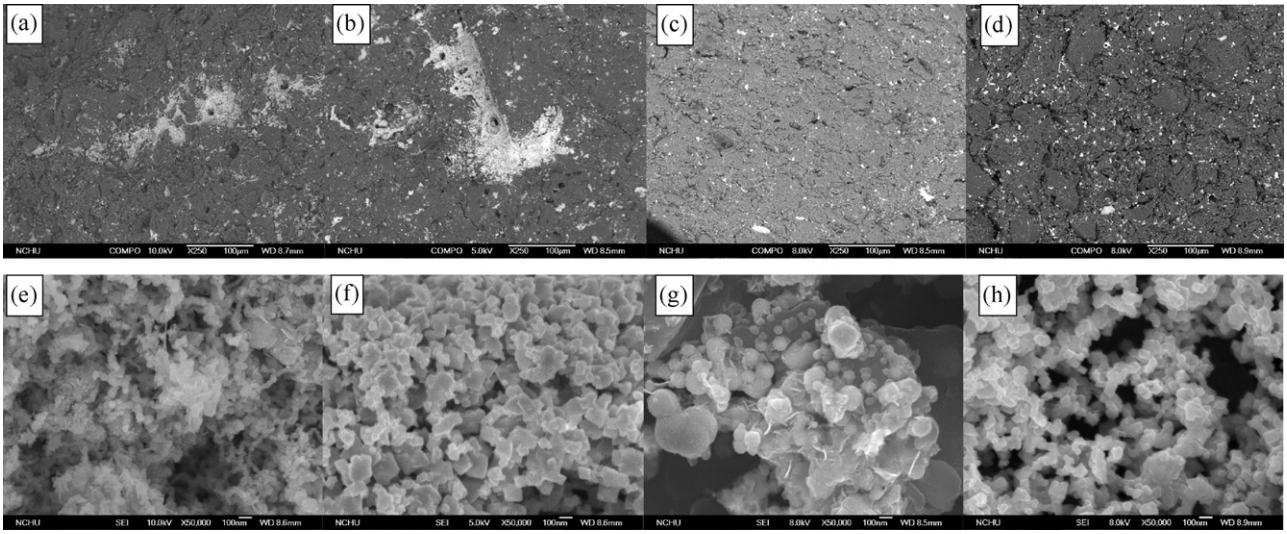

Fig. 1. SEM/BEI images of (a) GAC–ZVI105, (b) GAC–ZVI700, (c) GAC–ZVI105P and (d) GAC–ZVI700P composites; SEM/SEI images of (e) GAC–ZVI105, (f) GAC–ZVI700, (g) GAC–ZVI105P and (h) GAC–ZVI700P composites.

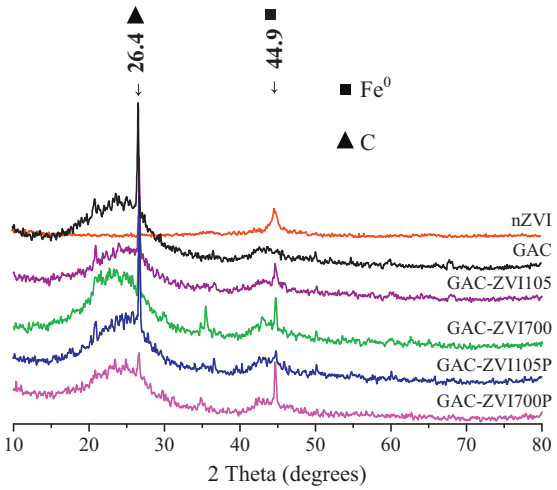

Fig. 2. XRD analysis of GAC–ZVI composites.

3.2. Adsorption and dechlorination behavior of the GAC–ZVI composites

Fig. 3 presents the results of adsorption and/or dechlorination of the TCE onto ZVI, GAC and GAC–ZVI composites. As can be seen, complete adsorption of TCE was achieved after around 300 min and partial TCE degradation using ZVI alone was also detected. The pseudo-first-order rate model for adsorption and/or dechlorination fits well to the TCE disappearance kinetics calculated where $R^2 > 0.97$. The pseudo-first-order rate constant ($k_{obs,TCE}$) data for TCE removal is presented in Fig. 3(a) and shows that the adsorption kinetics of the GAC–ZVI composites and the GAC when used alone were similar. Kim et al. [28] synthesized a ZVI immobilized cationic exchange membrane (CEM) for treating TCE and reported that the synthesized material exhibited a higher potential for TCE removal than the individual use of either CEM or ZVI. Therefore, it is speculated that the ZVI imbedded on the composite may react with TCE that has been sorbed onto the GAC and thus enhance TCE removal from the aqueous phase. Fig. 3(b) shows Cl variations during the course of the reaction in the aqueous phase. It can be seen that the usage of the GAC–ZVI composites resulted in more Cl liberations than the usage of ZVI alone. Furthermore, based on the analytical results of Cl liberation (assuming that 3 mol of Cl^- is liberated from every 1 mol of mineralized TCE), it is clear that TCE remained in solution and was still sorbed onto solids at the end of reaction (i.e., 360 min). Mass balance was conducted and the data can be seen in Fig. 3(c). 96% of the TCE was sorbed. However, when ZVI particles were used, no adsorption occurred, most of TCE remained in solution and approximately 1% of the TCE was transformed into Cl. In all the experiments where GAC–ZVI composites were used, the results show that the amount of sorbed TCE ranged between 56% and 69% of the initial TCE mass and that Cl liberation ranged between 2 and 11%. The undetermined amount of TCE resulting from the formation of byproducts and/or complexation between Cl and Fe to form byproducts such as $FeCl_2$ and $CHClFeCCl_2$ was not explored in this study [29]. It should be noted that even though intermediates were not examined in this study, TCE degradation pathways, mechanisms and byproducts have all been well reported on in literatures [30–34]. Overall, these results demonstrate that imbedded and dispersed ZVI particles are present in close proximity to sorbed TCE on the GAC and thus might increase ZVI reductive reactivity during the course of dynamic sorption/desorption processes. It should also be pointed out that the GAC–ZVI700P composite displayed a greater capacity for the reductive dechlorination of TCE.

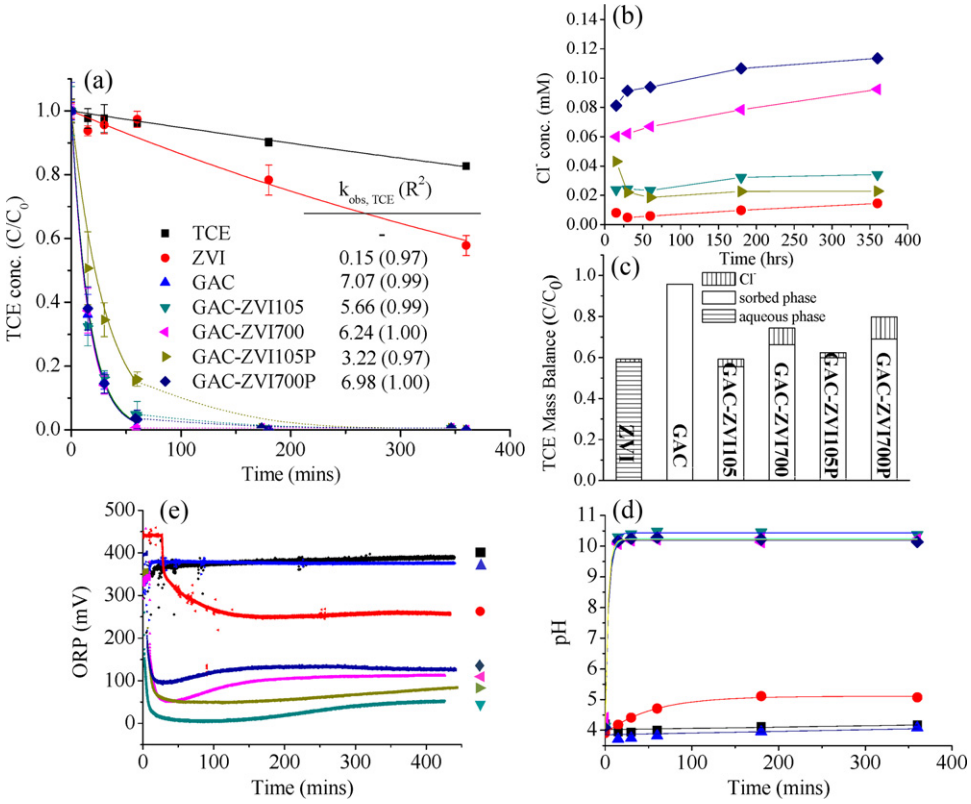

Fig. 3. (a) Disappearance kinetics of TCE adsorption and/or dechlorination onto ZVI, GAC and GAC–ZVI composites; (b) chloride ion variation; (c) TCE mass balance among sorbed and aqueous phases and chloride liberated after 360 min; (d) pH variation; (e) ORP variation. Reaction conditions: initial TCE 80 mg L^{-1}; 5 g L^{-1} GAC or GAC–ZVI composites; 0.15 g L^{-1} ZVI (note: 5 g L^{-1} composite × 3% (approximate iron content) = 0.15 g L^{-1}).

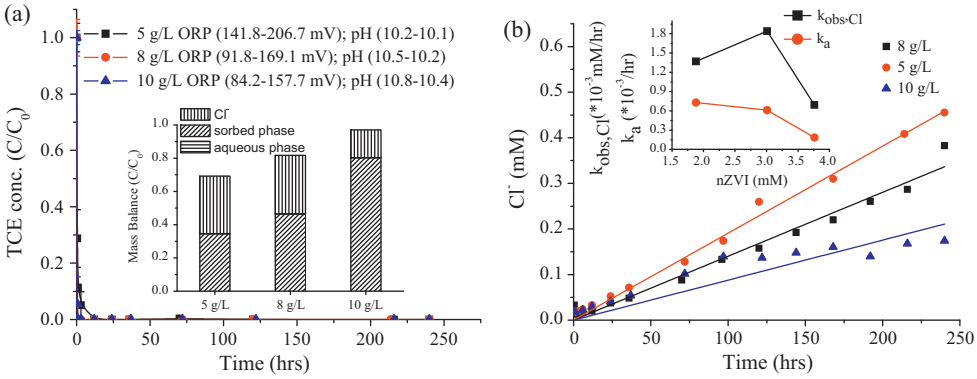

Fig. 4. (a) Disappearance kinetics of TCE adsorption and/or dechlorination onto the GAC–ZVI700P composite, inserted figure: mass balance among sorbed and aqueous phases and chloride liberated after 10 d; (b) chloride variation, inserted figure: $k_{obs,Cl}$ and k_a values as a function of imbedded ZVI contents on the GAC–ZVI700P composites. Reaction conditions: initial TCE 80 mg L^{-1}; 5, 8 and 10 g L^{-1} GAC–ZVI700P composites; imbedded ZVI content = weight of GAC–ZVI700P × 2.15%).

Additionally, Fig. 3(d and e) shows the variations in pH and ORP. The initial ORP in the solutions, which contained ZVI reveals a lag period that occurred due to an initial slow release of Fe^{2+} from the self-corrosion of ZVI [35]. Afterwards, ORP levels rapidly dropped to create a more reducing environment at around 250 mV and pH increased to around 5. Solutions which contained GAC–ZVI composites exhibited rapid drops in ORP to around 10–100 mV without a lag period and an increase in pH to around 10. Comparing ORP and pH in the presence of only ZVI, GAC and TCE, a more reducing environment and a higher pH were recorded when the GAC–ZVI composites were used. This is evidence of enhancement and maintenance of the dechlorination reaction by ZVI.

In the longer experiments (10 d) using the GAC–ZVI700P composites, different doses of the composite resulted in rapid removals of TCE from the aqueous phase, e.g., less than 1 h for 8 and 10 g L^{-1} dosages of GAC–ZVI700P (see Fig. 4(a)). As soon as the composites were added into the solutions, ORP dropped and pH increased to above 10. The usage of a higher dosage resulted in a more reducing environment and a more basic pH (data presented in Fig. 4(a)). The kinetics of TCE degradation using ZVI can be influenced by the concentration of ZVI and/or TCE and usually follows a pseudo-first-order kinetic model [29,32]. However, when the concentration of ZVI is a limiting factor in a reaction, i.e., when the concentration of TCE is higher or the ZVI dosage is lower, TCE degradation kinetics adhere to zero-order kinetics [34,36]. Therefore, when GAC–ZVI composites are used to treat TCE, the reaction mechanism includes simultaneous adsorption and dechlorination by GAC and ZVI, respectively. Concerning the dechlorination of TCE it is postulated that this would occur through ZVI degrading either sorbed TCE or dissolved TCE (desorbed from GAC under a condition of dynamic sorption/desorption equilibrium). Moreover, GAC adsorption attracts TCE, which then accumulates around ZVI imbedded in pores on the surface of the GAC. This may be regarded as an elevation in TCE mass which can then react with the limited amount of ZVI inside the GAC–ZVI composites, as discussed above, where adsorption is the dominant process during the initial stage of TCE removal. Hence, a zero-order Cl liberation reaction can be expected to occur following TCE dechlorination.

In the case of a heterogeneous reaction, i.e., employing GAC–ZVI, where the dechlorination rate-limiting step is a surface reaction (i.e., by ZVI), the rate of TCE degradation based on Langmuir–Hinshelwood's rate law can be given as [37]:

$$\frac{d[\mathrm{TCE}]}{dt} = \frac{-k_s S_t K_{\mathrm{TCE}}[\mathrm{TCE}]}{1 + K_{\mathrm{TCE}}[\mathrm{TCE}]} = -k_{\mathrm{obs}}[\mathrm{TCE}] \quad (2)$$

where k_s is the surface reaction rate constant ($mM^{-1}\,h^{-1}$); S_t is the total number of active sites (mM); K_{TCE} is the equilibrium constant for adsorption of TCE onto a reactive surface (mM^{-1}); [TCE] is the concentration of TCE that has been sorbed.

According to speculations presented above, the reactivity of GAC–ZVI is limited by the number of active ZVI sites. Hence, $K_{TCE}[TCE] \ll 1$ can be assumed and [TCE] sorbed can be regarded as a constant at an elevated concentration level [31,37]. Therefore, Eq. (2) can be modified to create Eq. (3).

$$\frac{d[\mathrm{TCE}]}{dt} = -k_s S_t K_{\mathrm{TCE}}[\mathrm{TCE}] = -k_a S_t = -k_{\mathrm{obs,Cl}} \quad (3)$$

where k_a is a desorption limited TCE degradation rate constant (h^{-1}); $k_{obs,Cl}$ is a zero-order Cl liberation rate constant (mM h^{-1}).

Fig. 4(b) shows the degree of Cl liberation over time and the inserted figure illustrates $k_{obs,Cl}$ where k_a is a function of the quantity of imbedded ZVI. $k_{obs,Cl}$ increased when the dose of the GAC–ZVI700P composite was increased from 5 to 8 g L^{-1}, but decreased when the dose was increased further to 10 g L^{-1}. These results demonstrate that an increase in the amount of GAC–ZVI composite resulted in a greater adsorption capacity than that of the interaction between ZVI and sorbed TCE. However, the k_a value, a desorption limited TCE degradation rate constant, decreased as the dose was increased. Adsorption occurred mostly onto GAC sites, while dechlorination occurred onto ZVI surface. Basically, the reaction mechanism might be in accordance with a sequence of adsorption, diffusion, and dechlorination in two heterogeneous GAC and ZVI materials. This trend indicates that Cl is liberated primarily via reduction of TCE by imbedded ZVI and that TCE degradation or mineralization is regulated by the degree of contact between TCE and ZVI during dynamic equilibrium that occurs between sorption and desorption.

At the end of the 10 d reaction, mass balance analysis was conducted and the results can be seen in the inserted figure in Fig. 4(a). As expected, the amount of residual TCE on the composite was the highest when 10 g L^{-1} of GAC–ZVI700P was used. Therefore, these results confirm that an increase in the dose of GAC–ZVI700P results in the rate of adsorption being higher than that of dechlorination. It was observed that a higher mass balance percentage was obtained using a higher dose of the composite, implying that more TCE had resided/sorbed on the composite, which was then available for solvent extraction. However, more chloride ions were detected in the aqueous phase under lower dose conditions. The GAC–ZVI700P composite can successfully retain TCE under all levels of dosages and subsequently create suitable conditions for imbedded ZVI to degrade TCE in either the sorbed (onto GAC adsorption sites) or dissolved phase (dissolved from GAC adsorption sites) close to ZVI.

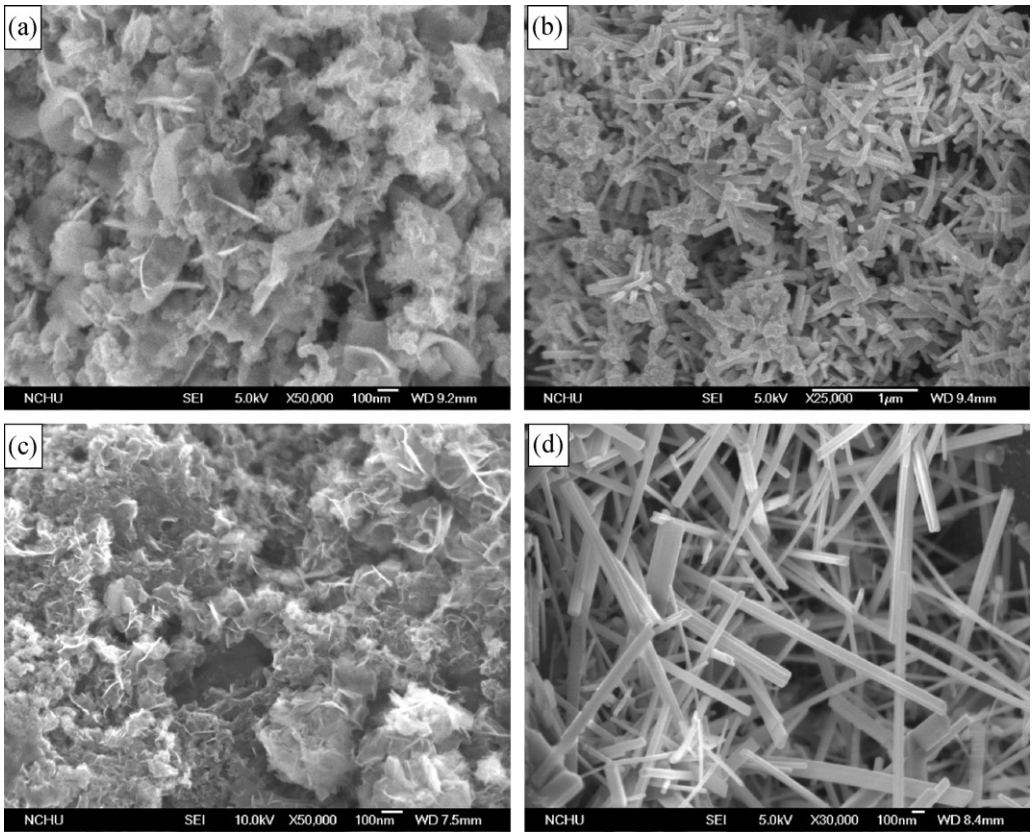

Fig. 5. SEM/SEI images of (a) GAC–ZVI105, (b) GAC–ZVI700, (c) GAC–ZVI105P, and (d) GAC–ZVI700P which were reacted for 10 d.

3.3. Observation of GAC–ZVI composites after reaction

SEM analysis of the changes which occurred on the surfaces of the composites was carried out and the results are shown in Fig. 5. Two distinct morphologies were observed: (1) acicular aggregate formations similar to cryptocrystalline clusters (in the absence and presence of PEG under calcination at a temperature of 105 °C, see Fig. 5(a and c)) [38,39] and (2) aggregated nanotubes (in the absence of PEG under calcination at a temperature of 700 °C, see Fig. 5(b)) or separated crystalline nanotubes (in the presence of PEG under calcination at a temperature of 700 °C, see Fig. 5(d)) [40]. It can be seen that the ZVI particles present on the GAC–ZVI composites that had been pretreated at 700 °C had become tubular by the end of the reactions. Moreover, it is apparent that the presence of PEG, which acts as a capping agent, is necessary for the formation of nanotube shapes (e.g., more separated).

Analysis of the XRD spectrum of GAC–ZVI composites that had been exposed to a TCE/water solution for 10 d (Fig. 6) reveals that magnetite (Fe_3O_4) and hematite (Fe_2O_3) were the two major corrosive products (identified based on standard JCPDS data) and that ZVI was still present. These observations are consistent with the findings of several studies, which investigated changes in the surface of ZVI during reductive reactions using TCE and identified the formation of iron oxides [34,35,41]. Interestingly, the Fe_2O_3 signals (at $2\theta = 52.0°$) are not visible and ZVI/Fe_3O_4 coupling appears to be dominant for the GAC–ZVI700P composite. Zhu et al. [42] reported that the majority of the iron oxide formed during the dechlorination of chlorobenzene on bimetallic Fe/Pd particles was Fe_3O_4. This could be due to the reduction of Fe_2O_3 to Fe_3O_4 by H_2, which is generated during the reduction of ZVI, in accordance with Eq. (4) [17]. Hence, it is speculated that surface corrosion of the ZVI was less extensive under a reducing condition induced by a more dispersed and imbedded ZVI. Note that Fe_3O_4 is considered crystalline at a 1:1 ratio of FeO (Fe^{2+}) to Fe_2O_3 (Fe^{3+}) and that the reduction of ferric oxide (i.e., Fe_2O_3) using gaseous reductants in industries follows the reductive reaction sequence $Fe_2O_3 \rightarrow Fe_3O_4 \rightarrow Fe^0$ [43]. Choi et al. [14] also reported that ZVI/Fe_3O_4 coupling could generate more electrons per unit of ZVI than ZVI/Fe^{2+}. This coupling may be the cause of the more complete degree of dechlorination, which was achieved using the GAC–ZVI700P composite.

$$3Fe_2O_3 + H_2 \rightarrow 2Fe_3O_4 + H_2O \quad (4)$$

The amount of Fe present on the surface of the composites after the 10 d reaction period are presented in Table 1. In general, the ZVI/iron oxide contents of the composites were highly stable. Only

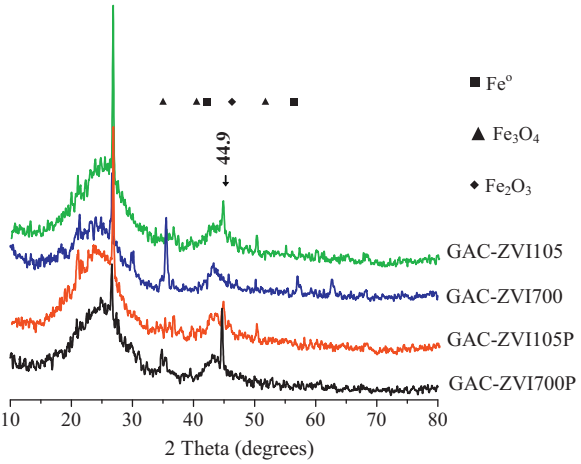

Fig. 6. XRD analysis of GAC–ZVI105, GAC–ZVI700, GAC–ZVI105P, and GAC–ZVI700P which were reacted for 10 d.

1% loss of Fe was lost from the composites treated at 700 °C (i.e., GAC–ZVI700 and GAC–ZVI700P), whereas losses of 10–15% were recorded when the other two composites were used. The stability of the ZVI/iron oxides was ascribed to their presence in GAC mesopores as described above.

4. Conclusion

The research project focused on enhanced the removal of TCE using GAC–ZVI composites which were synthesized to combine the advantages of a sorption material (GAC) and a reduction material (ZVI). When the GAC–ZVI composites were used in solution, ORP dropped more rapidly (to around 10–100 mV) and pH increase more (to 10) than when only ZVI was used. This is evidence of enhancement and maintenance of the dechlorination reaction by imbedded ZVI. Moreover, the imbedded and dispersed ZVI particles were present in close proximity to sorbed TCE on the GAC and thus increase the reductive reactivity of the ZVI during the course of the dynamic sorption/desorption processes. The GAC–ZVI700P composite that was prepared with the use of PEG at a higher calcination temperature (i.e., 700 °C) appeared to more completely disperse the ZVI particles than the other composites. When the GAC–ZVI composites were used to treat TCE, GAC adsorption attracted TCE which accumulated around ZVI imbedded in pores on the surface of the GAC. The TCE was then dechlorinated by ZVI, which degraded both sorbed and dissolved TCE. A zero-order chloride liberation reaction was observed to occur following TCE dechlorination. The GAC–ZVI composites combine the physical adsorption capacity of GAC with the dechlorination destructive reactivity of ZVI and can be used as a reactive GAC, which is not subject to the limitations of using GAC and ZVI separately.

Appendix A. Supplementary data

Supplementary data associated with this article can be found, in the online version, at doi:10.1016/j.jhazmat.2011.05.047.

References

[1] W.-X. Zhang, Nanoscale iron particles for environmental remediation: an overview, J. Nanoparticle Res. 5 (2003) 323–332.
[2] P.G. Tratnyek, R.L. Johnson, Nanotechnologies for environmental cleanup, Nano Today 1 (2006) 44–48.
[3] J. Zhan, T. Zheng, G. Piringer, C. Day, G.L. McPherson, Y. Lu, K. Papadopoulos, V.T. John, Transport characteristics of nanoscale functional zerovalent iron/silica composites for in situ remediation of trichloroethylene, Environ. Sci. Technol. 42 (2008) 8871–8876.
[4] L.J. Matheson, P.G. Tratnyek, Reductive dehalogenation of chlorinated methane by iron metal, Environ. Sci. Technol. 28 (1994) 2045–2053.
[5] S. Uludag-Demirer, A.R. Bowers, Gas phase reduction of chlorinated VOCs by zero valent iron, J. Environ. Sci. Health Part A 36 (2001) 1535–1547.
[6] L.B. Hoch, E.J. Mack, B.W. Hydutsky, J.M. Hershman, J.M. Skluzacek, T.E. Mallouk, Carbothermal synthesis of carbon-supported nanoscale zero-valent iron particles for the remediation of hexavalent chromium, Environ. Sci. Technol. 42 (2008) 2600–2605.
[7] T. Phenrat, N. Saleh, K. Sirk, R.D. Tilton, G.V. Lowry, Aggregation and sedimentation of aqueous nanoscale zerovalent iron dispersions, Environ. Sci. Technol. 41 (2007) 284–290.
[8] Z. Li, H.K. Jones, R.S. Bowman, R. Helferich, Enhanced reduction of chromate and PCE pelletized surfactant-modified zeolite/zerovalent iron, Environ. Sci. Technol. 33 (1999) 4326–4330.
[9] H. Zhang, Z.-h. Ji, L. Han, C.-h. Qin, Synthesis of nanoscale zero-valent iron supported on exfoliated graphite for removal of nitrate, Trans. Nonferrous Met. Soc. China 16 (2006).
[10] T. Zheng, J. Zhan, J. He, C. Day, Y. Lu, G.L. McPherson, G. Piringer, V.T. John, Reactivity characteristics of nanoscale zerovalent iron/silica composites for trichloroethylene remediation, Environ. Sci. Technol. 42 (2008) 4494–4499.
[11] J. Xu, D. Bhattacharyya, Modeling of Fe/Pd nanoparticle-based functionalized membrane reactor for PCB dechlorination at room temperature, J. Phys. Chem. 112 (2008) 9133–9144.
[12] G.K. Parshetti, R.-A. Doong, Dechlorination of trichloroethylene by Ni/Fe nanoparticles immobilized in PEG/PVDF and PEG/nylon 66 membranes, Water Res. 43 (2009) 3086–3094.
[13] H. Choi, S. Agarwal, S.R. Al-Abed, Adsorption and simultaneous dechlorination of PCBs on GAC/Fe/Pd: mechanistic aspects and reactive capping barrier concept, Environ. Sci. Technol. 43 (2009) 488–493.
[14] H. Choi, S.R. Al-Abed, S. Agarwal, Effects of aging and oxidation of palladized iron embedded in activated carbon on the dechlorination of 2-chlorobiphenyl, Environ. Sci. Technol. 43 (2009) 4137–4142.
[15] H. Jüntgen, Activated carbon as catalyst support: a review of new research results, Fuel 65 (1986) 1436–1446.
[16] M.J. Bonder, Y. Zhang, K.L. Kiick, V. Papaefthymiou, G.C. Hadjipanayis, Controlling synthesis of Fe nanoparticles with polyethylene glycol, J. Magn. Magn. Mater. 311 (2007) 658–664.
[17] H. Choi, S.R. Al-Abed, S. Agarwal, D.D. Dionysiou, Synthesis of reactive nano-Fe/Pd bimetallic system-impregnated activated carbon for the simultaneous adsorption and dechlorination of PCBs, Chem. Mater. 20 (2008) 3649–3655.
[18] X. Wen, S. Wang, Y. Ding, Z.L. Wang, S. Yang, Controlled growth of large-area, uniform, vertically aligned arrays of α-Fe_2O_3 nanobelts and nanowires, J. Phys. Chem. B 109 (2005) 215–220.
[19] W.-X. Zhang, D.W. Elliott, Applications of iron nanoparticles for groundwater remediation, Rem. J. 16 (2006) 7–21.
[20] W. Wang, Z.-H. Jin, T.-L. Li, H. Zhang, S. Gao, Preparation of spherical iron nanoclusters in ethanol–water solution for nitrate removal, Chemosphere 65 (2006) 1396–1404.
[21] A. Ghauch, A. Tuqan, H.A. Assi, Antibiotic removal from water: elimination of amoxicillin and ampicillin by microscale and nanoscale iron particles, Environ. Pollut. 157 (2009) 1626–1635.
[22] H.-J. Fan, I.-W. Chen, M.H. Lee, T. Chiu, Using FeGAC/H_2O_2 process for landfill leachate treatment, Chemosphere 67 (2007) 1647–1652.
[23] Y. Sun, M. Takaoka, N. Takeda, T. Matsumoto, K. Oshita, Kinetics on the decomposition of polychlorinated biphenyls with activated carbon-supported iron, Chemosphere 65 (2006) 183–189.
[24] C. Liang, Z.-S. Wang, C.J. Bruell, Influence of pH on persulfate oxidation of TCE at ambient temperatures, Chemosphere 66 (2007) 238–259.
[25] F. Rodriguez-Reinoso, The role of carbon materials in heterogeneous catalysis, Carbon 36 (1998) 159–175.
[26] A.B.M. Giasuddin, S.R. Kanel, H. Choi, Adsorption of humic acid onto nanoscale zerovalent iron and its effect on arsenic removal, Environ. Sci. Technol. 41 (2007) 2022–2027.
[27] Y. Xiong, J. Ye, X. Gu, Q. Chen, Synthesis and magnetic properties of iron oxide nanoparticles/C and α-Fe/iron oxide nanoparticles/C composites, J. Magn. Magn. Mater. 320 (2008) 107–112.
[28] H. Kim, H.-J. Hong, Y.-J. Lee, H.-J. Shin, J.-W. Yang, Degradation of trichloroethylene by zero-valent iron immobilized in cationic exchange membrane, Desalination 223 (2008) 212–220.
[29] J. Gotpagar, E. Grulke, T. Tsang, D. Bhattacharyya, Reductive dehalogenation of trichloroethylene using zero-valent iron, Env. Prog. 16 (1997) 137–143.
[30] A.L. Roberts, L.A. Totten, W.A. Arnold, D.R. Burris, T.J. Campbell, Reductive elimination of chlorinated ethylenes by zero-valent metals, Environ. Sci. Technol. 30 (1996) 2654–2659.
[31] W.A. Arnold, A.L. Roberts, Pathways and kinetics of chlorinated ethylene and chlorinated acetylene reaction with Fe(0) particles, Environ. Sci. Technol. 34 (2000) 1794–1805.
[32] W.S. Orth, R.W. Gillham, Dechlorination of trichloroethene in aqueous solution using Fe^0, Environ. Sci. Technol. 30 (1996) 66–71.
[33] T.J. Campbell, D.R. Burris, A.L. Roberts, J.R. Wells, Trichloroethylene and tetrachloroethylene reduction in a metallic iron–water–vapor batch system, Environ. Toxicol. Chem. 16 (1997) 625–630.
[34] Y. Liu, G.V. Lowry, Effect of particle age (Fe^0 content) and solution pH on NZVI reactivity: H_2 evolution and TCE dechlorination, Environ. Sci. Technol. 40 (2006) 6085–6090.
[35] C. Liang, M.-C. Lai, Trichloroethylene degradation by zero valent iron activated persulfate oxidation, Environ. Eng. Sci. 2008 (2008) 1071–1078.
[36] Y. Liu, S.A. Majetich, R.D. Tilton, D.S. Sholl, G.V. Lowry, TCE dechlorination rates, pathways, and efficiency of nanoscale iron particles with different properties, Environ. Sci. Technol. 39 (2005) 1338–1345.
[37] T. Kohn, W.A. Arnold, A.L. Roberts, Reactivity of substituted benzotrichlorides toward granular iron, Cr(II), and an iron(II) porphyrin: a correlation analysis, Environ. Sci. Technol. 40 (2006) 4253–4260.
[38] S.R. Kanel, B. Manning, L. Charlet, H. Choi, Removal of arsenic(III) from groundwater by nanoscale zero-valent iron, Environ. Sci. Technol. 39 (2005) 1291–1298.
[39] Y. Furukawa, J.-W. Kim, J. Watkins, R.T. Wilkin, Formation of ferrihydrite and associated iron corrosion products in permeable reactive barriers of zero-valent iron, Environ. Sci. Technol. 36 (2002) 5469–5475.
[40] P.S. Chowdhury, P.R. Arya, K. Raha, Synthesis and characterization of α-Fe_2O_3 nanoparticles of different shapes, Syn. React. Inorg. Met. 38 (2008) 212–216.
[41] K. Sohn, S.W. Kang, S. Ahn, M. Woo, S.-K. Yang, Fe(0) nanoparticles for nitrate reduction: Stability, reactivity, and transformation, Environ. Sci. Technol. 40 (2006) 5514–5519.
[42] B.-W. Zhu, T.-T. Lim, J. Feng, Influences of amphiphiles on dechlorination of a trichlorobenzene by nanoscale Pd/Fe: adsorption, reaction kinetics, and interfacial interactions, Environ. Sci. Technol. 42 (2008) 4513–4519.
[43] R.S. Treptow, L. Jean, The iron blast furnace: a study in chemical thermodynamics, J. Chem. Educ. 75 (1998) 43–47.